Caloric curve for the liquid-to-gas transition of the H_25^+ hydrogen cluster ion

F. Gobet, B. Farizon, M. Farizon, M.J. Gaillard, J.P. Buchet, M. Carre, T.D. Maerk

Caloric curve for the liquid-to-gas transition of the H_{25}^+ hydrogen cluster ion

F. Gobet [a], B. Farizon [a,*], M. Farizon [a], M.J. Gaillard [a], J.P. Buchet [b], M. Carré [b], T.D. Märk [c]

[a] *Institut de Physique Nucléaire de Lyon, IN2P3-CNRS et Université Lyon I, 43 boulevard du 11 Novembre 1918, F-69622 Villeurbanne Cedex, France*

[b] *Laboratoire de Spectrométrie Ionique et Moléculaire, CNRS et Université Lyon I, 43 boulevard du 11 Novembre 1918, F-69622 Villeurbanne Cedex, France*

[c] *Institut für Ionenphysik, Leopold Franzens Universität, Technikerstr. 25, A-6020 Innsbruck, Austria*

High energy collisions (60 keV/amu) of the H_{25}^+ hydrogen cluster ions with an helium target have been completely analyzed on an event-by-event basis in a recently developed multi-coincidence experiment. By selecting specific decay reactions we can start after the energizing collision with a microcanonical cluster ion ensemble of fixed excitation energy. From the respective fragment distributions for these selected decay reactions we derive corresponding temperatures of the decaying cluster ions. The relation between this temperature and the excitation energy (caloric curve) exhibits the typical prerequisites (plateau region) of a first order phase transition in a finite system, in the present case signaling the transition from a bound cluster to the free gas phase type situation.

Keywords: Phase transition; Caloric curve; Hydrogen cluster ions; Cluster fragmentation

1. Introduction

Phase transitions are universal properties of matter in interaction. They have been extensively studied in the thermodynamical limit of infinite system. However in many physical situations this limit cannot be accessed and so phase transitions should be reconsidered from a more general point of view. This is for example the case of matter under long range forces like gravitation [1]. Even if these self gravitating systems are very large they cannot be considered as infinite system because of the nonsaturating nature of the force. Other cases are provided by microscopic or mesoscopic systems consisting of matter which is known to exhibit phase transitions. Metallic clusters can melt before being vaporized [2,3]. Quantum fluid may undergo Bose condensation or super-fluid transition [4]. Dense hadronic matter should merge in a quark-gas phase transition [5]. One of the great challenges in cluster physics in the last years was the identification and characterization of critical behavior and the observation of phase transitions, including solid-to-liquid and liquid-to-gas phase transitions. Since clusters are particles of finite size one is confronted with the general question of how to detect and/or characterize such a transition in a finite system.

* Corresponding author. E-mail: bfarizon@ipnl.in2p3.fr

It has been proposed that phase transitions in finite systems within the microcanonical ensemble [1,6] may be detected by a characteristic functional relationship between the temperature and the excitation energy, the so-called caloric curve, i.e., a first order phase transition should correspond to a negative branch for the heat capacity [7–9].

In a strict sense, sharp second order phase transitions can only occur in the thermodynamic limit that is critical singularities are only present for a system with a large number of particles [10]. In small systems such as two colliding nuclear or molecular systems fluctuations may wash out the signature of the phase transition [8,11]. Nevertheless, it has been demonstrated theoretically (see [11] and references therein) and also experimentally (see [12] and references therein) that finite systems may indeed exhibit a critical behavior to be seen when studying inclusive fragment size distributions, scaled factorial moments, and anomalous fractal dimensions. For instance recent heavy ion collision experiments around the Fermi energy (see ref. [9] in [11]) and cluster collision experiments around the Bohr energy (see [13] and references therein) have shown the formation of many different fragments in the exit channel of the reaction exhibiting a power law in total fragment size distributions. Such a power law, as described by the Fisher droplet model [14,15] is expected to hold for droplet condensation/evaporation near the critical temperature, indicating a liquid-to-gas second order phase transition. However, recent work on the lattice gas model [8] demonstrates that a critical behavior is compatible with a first order phase transition because of the finite size effects. As concluded by Gross and coworkers [6,16] on the basis of extensive theoretical modeling the best signature, however, of a phase transition of first or second order in a finite system is the specific shape of the caloric curve (see [7,9]) or according to the theoretical work of Berry and coworkers [17–19] the specific dependence of the thermodynamic temperature on the total energy in the system.

Pochodzolla et al. [20] were the first to determine experimentally a relation between the temperature of hot decaying nuclei resulting from Au + Au collisions at 600 MeV/amu and their excitation energy, the shape of this relation exhibiting the characteristic plateau expected for a phase transition. The validity of this first experimental observation of a caloric curve for a liquid-to-gas phase transition for nuclear systems (in particular the determination of the temperature) was later questioned [8] because follow-up experiments arrived at different shapes (see [21,22] and references therein). On the other hand, Haberland and coworkers [2,3,23] reported the first experimental determination of a caloric curve for the solid-to-liquid like transition (melting) of a small cluster temperature, i.e., a sodium cluster consisting of 139 atoms [2]. A beam of cluster ions was generated with a canonical distribution of internal energy thus fixing the temperature. One cluster size was selected (thus switching to microcanonical system), irradiated by photons and the photofragmentation pattern (which can be related to the energy) was measured as a function of this cluster temperature. Moreover, Bachels et al. [24] reported recently a caloric curve for the melting of a free tin cluster distribution (without mass selection) employing a sensitive pyroelectric foil, the interpretation of their experiment was, however, later questioned [25]. Very recently Schmidt et al. [26] reported a caloric curve for $Na_{139}{}^{+}$ measured from 100 K up to the temperature where the clusters are boiling and spontaneously emit atoms thereby allowing them to construct the caloric curve across the liquid to gas change for a sodium cluster ion. Moreover, we were recently able, employing an advanced accelerator mass spectrometry experiment [27], to derive for the first time the relation between the temperature and the excitation energy (caloric curve) for a molecular cluster ion (e.g., the $H_{27}{}^{+}$ ion). This relation exhibited the typical prerequisites of a first order phase transition in a finite system signaling the transition from a bound cluster to the gas phase [27]. In the present paper we extend our previous study to another cluster ion, i.e., the $H_{25}{}^{+}$ ions. It has to be noted that the sizes of these hydrogen cluster ions are much smaller than the previously studied metal cluster ions and thus we are probing here the lower limit of the underlying statistical concept.

The protonated hydrogen cluster ions represent in contrast to the previously studied metal cluster ions [23–26] a quite different class of systems where a quantum solute is solvated by a quantum solvent; the added proton becomes trapped and a tightly localized H_3^+ core is surrounded by solvating H_2 molecules, $H_3^+(H_2)_{m=11}$ [28]. Moreover, after the energizing collisions between 60 keV/amu ions with a helium target we select a microcanonical ensemble of cluster ions with a given energy (by selecting specific decay reactions from a host of possible decay channels) and determine from the (partial) fragment size distribution the corresponding temperature of the ensemble of decaying cluster ions. This experiment involves the complete event-by-event analysis of 11,685 collisions using a recently developed [12,13] multi-coincidence technique for the simultaneous detection of the correlated, ionized and neutral, collision fragments thus allowing us to obtain an experimental caloric curve for the transition from a bound cluster to the gas phase.

2. Experimental set-up

Mass selected hydrogen cluster ions with an energy of 60 keV/amu are prepared in a high-energy cluster ion beam facility [12] consisting of a cryogenic cluster jet expansion source combined with a high performance electron ionizer and a two step ion accelerator (consisting of an electrostatic field and a RFQ post-accelerator). After momentum analysis by a magnetic sector field, the mass selected high energy projectile pulse (pulse length 100 ms, repetition frequency 1 Hz) consisting in the present study of $H_3^+(H_2)_{m=11}$ cluster ions is crossed perpendicularly by a helium target beam effusing from a cylindrical capillary tube (see Fig. 1). Prior to this the ion beam is collimated by two apertures ensuring an angular dispersion of about ± 0.8 mrad. One meter behind this collision region the high energy hydrogen collision products (neutral and ionized) are passing a magnetic sector field analyzer. The undissociated primary $H_3^+(H_2)_{m=11}$ cluster projectile ion or the neutral and charged fragments resulting from reactive collisions are then detected approximately 0.3 μs after the collision event with a multi-detector device consisting of an array of passivated implanted planar silicon surface barrier detectors located at different positions at the exit of the magnetic analyzer.

With this instrument we are able to record for each event simultaneously the number (multiplicity) of each mass-identified fragment ion resulting from the interaction (for more experimental details, see [12,13,29]). In addition, for each event we can also monitor in coincidence with the detected ions the sum of the masses of all the neutral fragments. Moreover, by probing the angular distribution of these neutrals in front of the detector by using a movable aperture (0.5 mm of diameter) and additional information (as described later) about the reaction probability of H_2 and H_3^+ projectiles we can conclude that the neutral products observed consist only of hydrogen atoms and hydrogen molecules [30] with no larger neutral clusters present. As an example, we report in Fig. 2a the spectrum corresponding to the detection of all the neutral fragments produced by collisions of H_{15}^+ cluster ions with helium target atoms

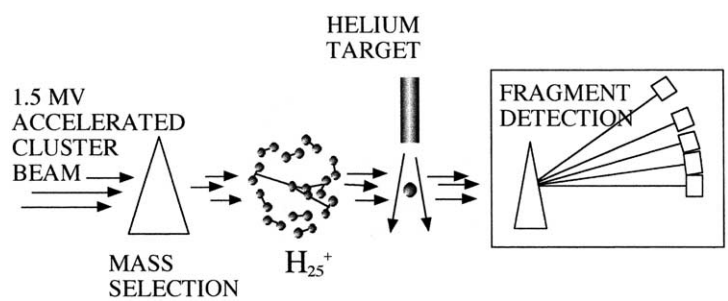

Fig. 1. Schematic view of the experimental set-up.

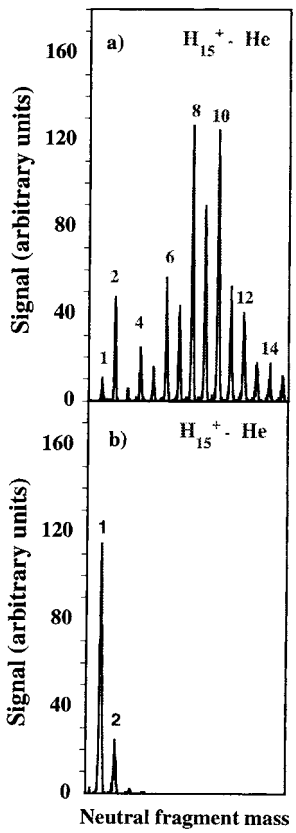

Fig. 2. Mass spectrum for the neutral fragments for decaying H_{15}^+ ions: (a) without movable collimator in front of the detector and (b) with movable collimator in front of the detector.

without using this moveable collimator. The number associated with each peak in this figure corresponds to the measured total neutral mass being produced in a single collision by one fragmenting cluster ion H_{15}^+. We observe 15 separate peaks (as described in detail in reference [31]) the peak at the lowest mass corresponding to an hydrogen atom with mass 1 amu and the peak at the highest mass corresponding to a total mass of 15 amu. Without further measurements we cannot at this point identify the identity of the neutrals causing these peaks, e.g., the peak at mass 4 could be due to four hydrogen atoms, two hydrogen molecules, two hydrogen atoms plus one hydrogen molecule or to one hydrogen dimer $(H_2)_2$. One way to obtain more information is to measure the neutral fragments under the same experimental condition however with the movable collimator positioned in front of the dectector for the neutral fragments thereby limiting the acceptance angle for neutral fragments being produced in the collision region by a single collisional event. In this case (see Fig. 2b) only two major peaks can be observed in the spectrum one at mass 1 and one at mass 2, respectively, corresponding to the detection of H, H + H or H_2. This immediately excludes the possibility that neutral fragments larger than H_2 are being produced by these collisions. The reason that we do see larger peaks when removing this collimator is due to the fact that in this case we can detect several neutral fragments from one collision event even if these fragments are produced with initial kinetic energy and thus have spread over a large area at the point of detection (with the collimator we will detect only the central part of the beam, and if we do not detect larger masses than 2 we can safely conclude that no larger molecules are present in the beam). Nevertheless, we also observe in Fig. 2b a few events corresponding to mass 3 and 4. The diameter aperture has been chosen in such a way that the probability to detect simultaneously two fragments originating from the same fragmenting cluster (e.g., one leaving the fragmenting cluster ion in forward and one in backward direction) is very small. But this probability cannot be reduced to zero and thus we are expecting a few events with larger masses even if the largest fragment is H_2. Thus mass 3 may be interpreted as being due to the simultaneous detection of one hydrogen atom and one hydrogen molecule (there exists no neutral hydrogen trimer) and mass 4 may be interpreted as being mainly due to the simultaneous detection of two hydrogen molecules. One additional reason why the peak at mass 4 cannot be interpreted as evidence for the existence of bound neutral fragment $(H_2)_2$ is the rather high multiplicity observed for the neutral fragments produced (see the large signal for the higher mass numbers in Fig. 2a).

So far we have therefore determined that fragments produced (and detected with the collimator) have mass 1 or 2. In order to obtain information about the identity of the detected signal at mass 2 one needs further information. This may be obtained by using a movable

grid in front of the detector and studying the reaction probabilities for H_2 and H_3^+ projectiles interaction with a He target. This allows us to distinguish whether a resulting signal at a mass of 2 amu is due to one hydrogen molecule, due to two hydrogen atoms or due to a certain mixture of these two cases (for details of this rather involved analysis see [30,32]). For larger clusters this technique cannot be directly applied and therefore additional information on relative cross sections for the various product channels needs to be used for a complete analysis of the neutral mass peak [30].

Thus without going here into further experimental detail we can state that we are able to analyze on an event-by-event basis the identity of all correlated fragments produced in a single collision event between the $H_3^+(H_2)_{11}$ cluster ion and the He target atom, the fragmentation reactions having the general form

$$\begin{aligned} &H_3^+(H_2)_{11}+He \\ &\quad\rightarrow a H_3^+(H_2)_k + b H_3^+ + c H_2^+ + d H^+ \\ &\qquad + e(H_2) + f H \quad \text{with } a\text{–}f = 0, 1, \ldots . \end{aligned} \tag{1}$$

The validity of single collision conditions has been ascertained by measurements at different He target pressures and allows us to derive also absolute cross sections for the occurrence of specific reaction channels (partial cross sections, for details see [33]). This complete analysis allows us to go beyond the straightforward determination of total fragment size distributions as reported previously ([13] and references therein), since we are able to generate for the first time partial fragment size distributions for selected decay reactions or classes of decay reactions.

3. Construction of the caloric curve

As we need for the construction of a caloric curve the simultaneous determination of the energy and the temperature of the system, we use the ability to select certain classes of reactions to group our analyzed events into a number of different subgroups each representing collisions in which a certain amount of energy is deposited into the cluster. Thus we are generating from our large set of collisions various subsets containing only cluster ions with a certain energy (or energy range) in a microcanonical sense. The basic idea behind this is to analyze each decay reaction in terms of the energy required for all the particles produced in such a decay reaction (taking into account the well known potential energy curves for the hydrogen molecule when calculating the energy for the Franck–Condon transitions from quasi-isolated cold ground state H_2 molecules to the various excited states involved) and to use the total energy value obtained as a measure for the internal energy prior to the decay.

For instance, analyzing the identity of the neutrals the observed decay reactions of $H_3^+(H_2)_{11}$ ions into $H_9^+ + H_2^+$ plus a neutral mass totaling 14 amu shows that 86.1% of the cases correspond to the production of seven hydrogen molecules. In this case the necessary energy for the reaction is 15.7 eV (the ionization energy for the hydrogen molecule) neglecting the much smaller binding energy of the hydrogen molecules. Similarly, 13% of these events correspond to the production of six hydrogen molecules and two hydrogen atoms necessitating an additional energy input of about 10.3 eV to dissociate one molecule into two atoms (thus yielding a total energy of 26 eV), 0.8% correspond to five molecules and four atoms (total energy of 36.3 eV) and 0.1% to four molecules and six atoms (total energy of 46.6 eV).

Fig. 3 shows for the $H_3^+(H_2)_{m=11}$ cluster ion projectile the corresponding measured partial fragment mass distribution for eight selected subsets each of which includes reactions of a certain energy range, e.g., 2–12 eV, 15–25 eV, etc. It is interesting to note that the shape of these distributions changes significantly as a function of the energy deposited, i.e., from a U-shaped form at low energy which is due to the occurrence of a mixture of evaporation and multi-fragmentation processes, to a pure power law at intermediate energies due to the presence of only multi-fragmentation reactions to finally a regime at high energies which is dominated by complete disintegration processes. So far these different regimes could only be observed by different experiments with widely different collision parameters ranging from low energy mass spectrometer collision experiments [34], to high

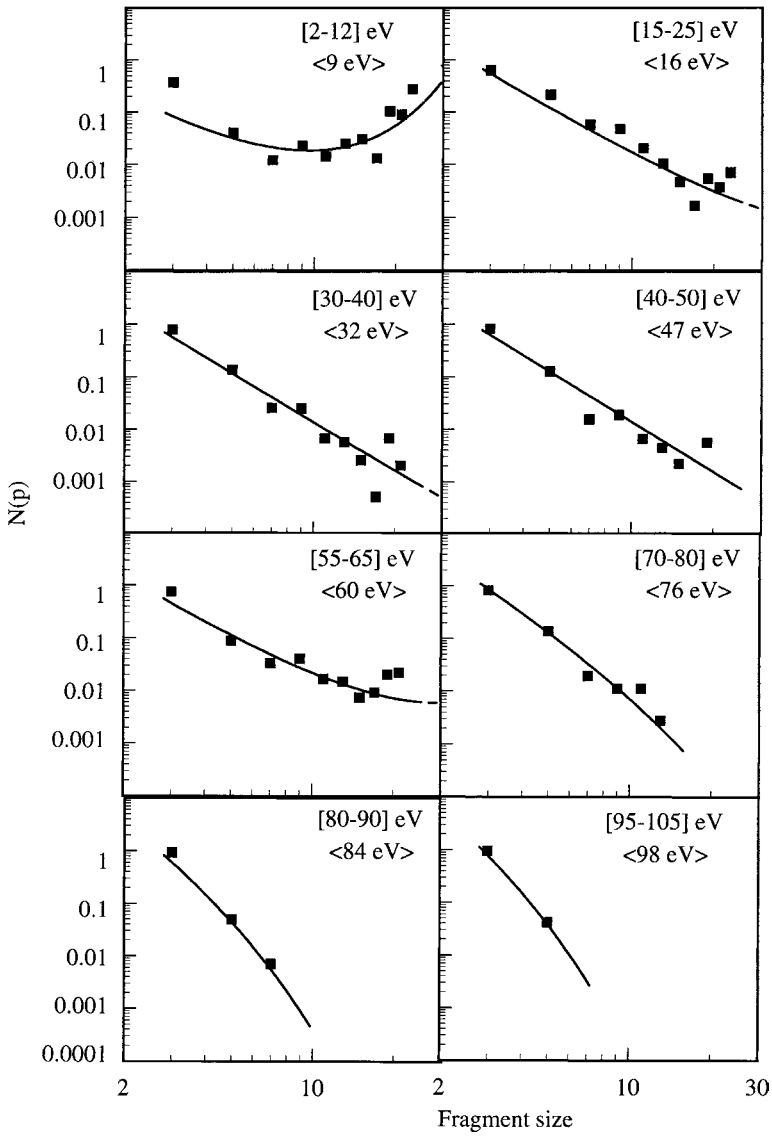

Fig. 3. Partial fragment mass distributions for different subsets of reaction channels (selected according to the energy deposited in the collision complex, i.e., 2–12 eV, 15–25 eV, etc.) occurring in collisions of 60 keV/amu H_{25}^+ ions with He. Solid lines: fits using Fisher's formula (see text).

energy cluster/atom or nuclear collision experiments (see [13] and references therein) and to beam foil experiments with clusters yielding only atomic fragment ions [35]. This is the first time (see also recent results reported for the H_{27}^+ cluster ion [27]) that this characteristic change of the mass distribution as a function of energy deposited has been determined in only one experiment over the whole range of possible shapes and thus possible decay mechanisms.

Returning now to the construction of the caloric curve we need in a second step to determine for each subset of known energy the corresponding temperature of the cluster ions prior to the decay. Here we use a relationship between the characteristic shape of a

fragment mass distribution and the temperature of the decaying nuclei at around the critical point reported recently by Belkacem et al. [11]. They were able to fit quite differing numerical mass distributions obtained by classical MD calculations for a nucleus with 100 constituents (see the distributions shown in Fig. 4) at different initial canonical temperatures (by generating 2000 events per temperature) very well with Fisher's droplet formula [14]

$$\frac{\mathrm{d}N}{\mathrm{d}A} = Y_0 A^{-\tau} (X^A)^{2/3} Y^A, \tag{2}$$

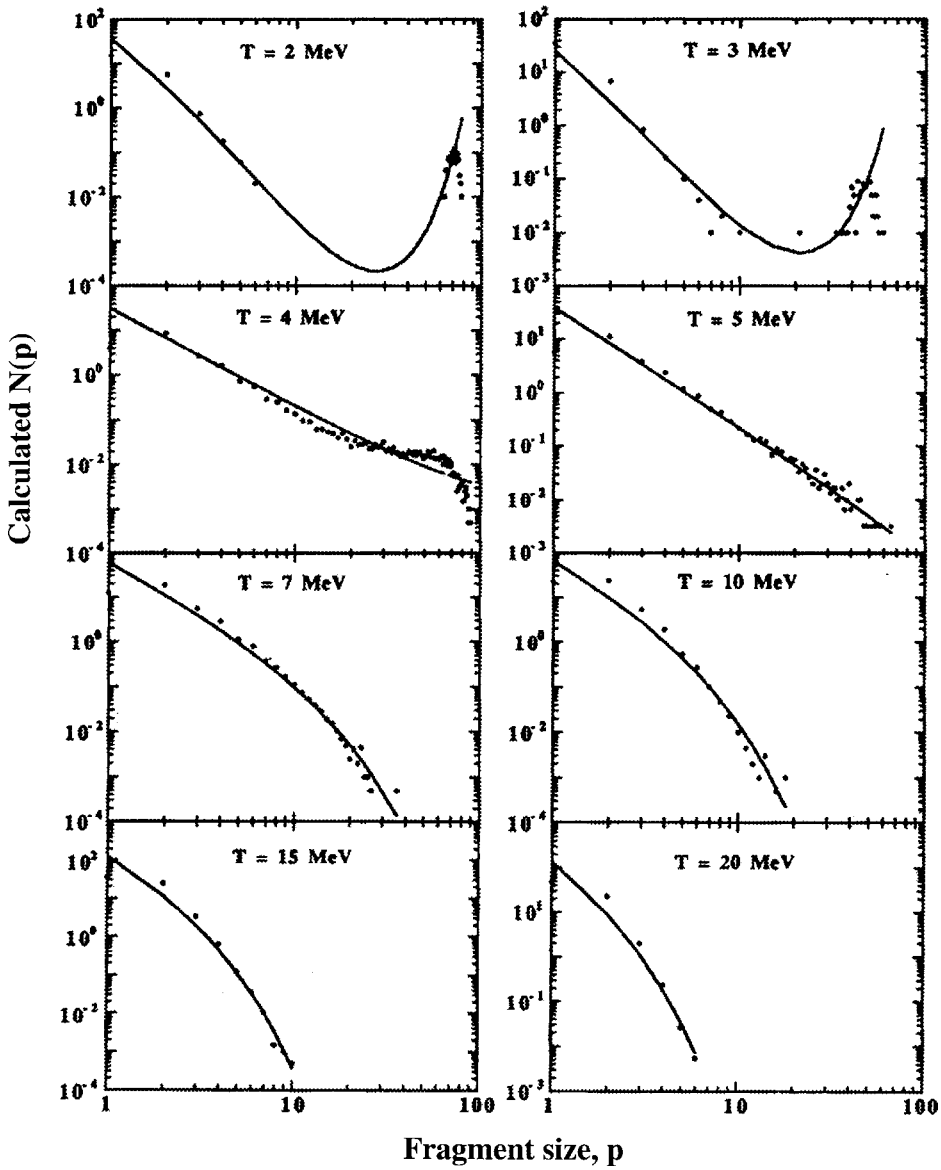

Fig. 4. Mass distributions obtained for the expansion of a nuclear system consisting of 100 constituents ($A = 100$) for eight different initial temperatures ranging from 2 to 20 MeV. The dots in the plot show the results of the MD calculations and solid lines the fits using Fisher's formula (adapted from Belkacem et al. [11]).

with Y_0, X, Y and τ fitting parameters and A the atomic mass number, thus demonstrating a direct relationship between the shape of the mass distribution (as described by (2) and in particular by the parameter Y which is related to the temperature approaching the value 1 at the critical temperature) and the initial temperature of the decaying system (see also [36]). In Fig. 4 we show the mass distributions and the corresponding fits obtained in this way for the expansion of the nuclear system with 100 constituents ($A = 100$) for eight different initial temperatures ranging from 2 to 20 MeV (from Belkacem et al. [11]). It is interesting to note at this point that these mass distributions exhibit a similar evolution of the fragment size distribution with increasing temperature as the present ones (see Fig. 3) with increasing amount of excitation energy.

Thus, following the methodology of Belkacem et al. [11] in fitting their mass distribution, i.e., first fixing the parameter τ using a rather pure power law distribution (e.g., the one at an energy of 47 eV in Fig. 4) and then fitting the other parameters by using all distributions (and doing this in an iterative way several times), we also succeeded to fit the presently obtained (partial) fragment mass distributions with Eq. (2). With a slope of -3.16 (as compared to -2.23 in the calculation of Belkacem et al. [11]; previous experimentally determined values for total fragment mass distribution for clusters and nuclei having values of about -2.6 [14]) we obtain a very good agreement between our experimental points and the fits (solid lines in Fig. 3; the corresponding values of the fitting parameters Y_0, X, Y and τ entering in the formula Eq. (2) are given in Table 1). In the case of the $H_3{}^+(H_2)_{m=12}$ [27] we used a slope of -3.38 and the fits obtained were equally convincing. This then allows us by comparison with the results of Belkacem et al. [11] (Fig. 4) to designate for each of the subsets considered a relative measure for the temperature due to the characteristic shape of its fragment mass distribution (as expressed by the fitted parameters, in particular the parameter Y).

Thus the major overriding conclusion for these results is that for small energies the distribution is quickly changing with increasing energy from a U-shaped form to a single power law fall off. Moreover, this power law, containing fragments of all sizes, is sustained over a broad energy range and thus this is direct evidence for a constant temperature in this energy range. Finally, at very large energies this power law is replaced by a shape which is falling off much faster than this power law signaling a sudden change (increase) in temperature. It is interesting to note that in a similar fashion, though in a different context and by different theoretical means, temperatures of decaying carbon cluster ions have been determined by measuring either the microcanical decay rate constants for monomer evaporation [37] (see also results for aniline-argon clusters [38], the kinetic energy release distributions for monomer evaporation [39] or the fragmentation pattern in surface-induced dissociations [40]). Using this 'temperature' which is only a relative measure (due to the comparison with MD calculations applied to the nuclear matter), we plot in Fig. 5 the temperature derived in reduced units vs. the energy deposited. As a matter of fact we have for this purpose considered more data subsets than shown in Fig. 3. Moreover, similar results have also been obtained for other cluster ion as shown in

Table 1
Values of the fitting parameters Y_0, X, Y, and τ entering in the Fisher formula Eq. (2) as derived from the experimental data for $H_{25}{}^+$ cluster ions shown in Fig. 3

$\langle E \rangle$	9 eV	16 eV	32 eV	47 eV	60 eV	76 eV	84 eV	98 eV
Y_0	1.0	14.9	17.7	20.1	10.6	42.1	87.7	211.3
X	1.00	1.00	1.00	1.00	1.00	1.00	1.00	1.00
Y	1.391	1.051	1.009	1.013	1.115	0.869	0.601	0.495
τ	3.16	3.16	3.16	3.16	3.16	3.16	3.16	3.16
T/T_0	0.88	0.99	1.045	1.0	0.97	1.755	2.96	3.45

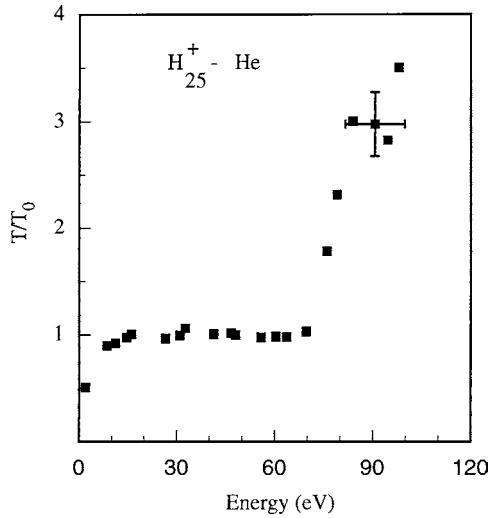

Fig. 5. Caloric curve for cluster fragmentation: temperature (given in reduced value (T/T_0), with T_0 the temperature in the plateau part of the curve) vs. the energy deposited in the H_{25}^+ cluster ion. The error bars given for one of the experimental points comprises on the one hand the maximum error in assigning the energy including the unknown extent of vibrational excitation in the one hydrogen molecule hit on average by the He atom during the collision and on the other hand the maximum error in assigning the temperature using various fitting procedures. In practice as we are using the best fit method for all the points the relative error in the temperature is much smaller and this is also mirrored by the rather small deviations of the experimental points from each other in the plateau region. This interpretation is confirmed by similar observations for other cluster sizes.

reference [27] thus confirming independence of this characteristic result from the finite particle size.

4. Results and conclusion

This caloric curve can be clearly divided into three parts, after an initial increase a distinct plateau is present before the curve is rising again. This curve therefore agrees qualitatively with the typical prerequisites of a first order phase transition [7] (see also Fig. 7 in [9]) in a finite system. It thus constitutes a strong signature for a liquid-to-gas like phase transition in a fragmenting cluster and thus confirms and replaces the other fingerprints such as the power law in mass distributions and factorial moment analyses [16]. As in the calculations discussed by Gross et al. [6] using microcanonical metropolis sampling for hot atomic metal clusters the transition occurs and is characterized by the interplay and transition from monomer evaporation reactions (see also Fig. 4) to multi-fragmentation reactions and complete vaporization events in this bound-free transition regime. The particular long plateau (indicating a relatively large apparent specific heat involved in this transition also observed for the melting of sodium cluster ions by Haberland and coworkers [2,3,23,26]) may be attributed to the many different degrees of freedom available in this special type of cluster being bound by a mixture of dispersion force (intermolecular binding) and covalent binding with more intramolecular excited states available than in atomic clusters.

Acknowledgements

Work supported by the FWF, Wien, Austria, the Amadee program of the French and Austrian governments and the EU Commission, Brussels.

References

[1] W. Thirring, Z. Phys. 235 (1970) 339.
[2] M. Schmidt, et al., Phys. Rev. Lett. 79 (1997) 99.
[3] M. Schmidt, et al., Nature 393 (1998) 238.
[4] Proceedings of "Quark Matter 1997", Nucl. Phys. A638 (1998) 1c.
[5] P.J. Siemens, Nature 305 (1983) 410;
M.W. Curtin, H. Toki, D.K. Scott, Phys. Rev. Lett. B123 (1983) 289.
[6] D.H.E. Gross, Phys. Rep. 279 (1997) 119. and references therein.
[7] P. Chomaz, F. Gulminelli, Phys. Rev. Lett. 85 (2000) 3587.
[8] F. Gulminelli, P. Chomaz, Phys. Rev. Lett. 82 (1999) 1402.
[9] P. Chomaz, et al. Proceedings of the XXXVIII International Winter Meeting on Nuclear Physics, Ricerca Scientifica ed Educazione Permanente supplemento 116 (2000) 336.
[10] P. Chomaz, F. Gulminelli, Nucl. Phys. A647 (1999) 153.
[11] M. Belkacem, et al., Phys. Rev. C52 (1995) 271.
[12] B. Farizon, et al., Phys. Rev. Lett. 81 (1998) 4108.
[13] B. Farizon, et al., Int. J. Mass Spectrom. Ion Processes 164 (1997) 225.
[14] M.E. Fisher, Rep. Prog. Phys. 30 (1967) 615.
[15] J.E. Finn, et al., Phys. Rev. Lett. 49 (1982) 1321.
[16] A.S. Botvina, D.H.E. Gross, Phys. Lett. B408 (1997) 31.
[17] D.J. Wales, R.S. Berry, Phys. Rev. Lett. 73 (1994) 2875.

[18] A. Proykova, R.S. Berry, Z. Phys. D40 (1997) 215.
[19] R.E. Kunz, R.S. Berry, Phys. Rev. Lett. E49 (1994) 1895.
[20] J. Pochodzolla, et al., Phys. Rev. Lett. 75 (1995) 1040.
[21] Y.G. Ma, et al., Phys. Rev. Lett. B390 (1997) 41.
[22] M. D'Agostino, et al., Nucl. Phys. A650 (1999) 329.
[23] R. Kusche, et al., Eur. Phys. J. D9 (2000) 1.
[24] T. Bachels, et al., Phys. Rev. Lett. 85 (2000) 1250.
[25] K. Kofman, et al., Phys. Rev. Lett. 86 (2001) 1388.
[26] M. Schmidt, et al., Phys. Rev. Lett. 87 (2001) 203402.
[27] F. Gobet, et al., Phys. Rev. Lett. 87 (2001) 203401.
[28] B. Farizon, et al., Phys. Rev. Lett. B60 (1999) 3821.
[29] B. Farizon, et al., Eur. Phys. J. D5 (1999) 5.
[30] F. Gobet, Analysis of the neutral fragments, Thèse de doctorat, Université Lyon 1, 2001.
[31] B. Farizon, et al., Int. J. Mass Spectrom. Ion Processes 144 (1995) 79.
[32] G. Jalbert, et al., Phys. Rev. Lett. A47 (1993) 4768.
[33] B. Farizon, et al., Nucl. Instrum. Methods Phys. Res. B101 (1995) 287.
[34] A. Van Lumig, J. Reuss, Int. J. Mass Spectrom. Ion Phys. 27 (1978) 197.
[35] B. Mazuy, et al., Nucl. Instrum. Methods Phys. Res. B28 (1987) 497.
[36] V.N. Kondratyev, H.O. Lutz, Z. Phys. D40 (1997) 210.
[37] H. Hohmann, et al., Z. Phys. D33 (1995) 143.
[38] P. Parneix, et al., J. Chem. Phys. 239 (1998) 121.
[39] S. Matt, et al., J. Chem. Phys. 113 (2000) 616.
[40] T. Fiegele, et al., Chem. Phys. Lett. 316 (2000) 387.